ENGINEERING Agriculture

Engineering Journals

RESEARCH ARTICLE

2026 / Volume 13 / Issue 4 / 26668

# Coupling mechanisms of electrophysiology and photosynthesis mediated by ion dynamics in high-voltage electrostatic field-regulated tomato seedling growth

**Ruijie XIE[1], Yanbo SONG[2], Xiaojing SHI[3], Liyan JIA[3], Zhenyu LIU (✉)[4,5]**

1 Department of Big Data and Intelligent Engineering, Shanxi Institute of Technology, Yangquan 045000, China.
2 College of Life Sciences, Shanxi Agricultural University, Taigu 030801, China.
3 College of Food Science and Engineering, Shanxi Agricultural University, Jinzhong 030801, China.
4 College of Agricultural Engineering, Shanxi Agricultural University, Taigu 030801, China.
5 Dryland Farm Machinery Key Technology and Equipment Key Laboratory of Shanxi Province, Taigu 030801, China.

**KEYWORDS**

High-voltage electrostatic field, ionic composition, ionic transport rate, photosynthesis, tomato growth

**HIGHLIGHTS**

- A positive high-voltage electrostatic field (+HVEF) was found to significantly promote the growth and development of tomato seedlings.
- Distribution of ions in roots, stems and leaves was systematically elucidated.
- +HVEF enhanced the mechanical strength of tomato seedling stems.
- $Mg^{2+}$ transport induced by +HVEF promotes chlorophyll synthesis and photosynthesis.
- Integration of electrical and physiological analyses reveals electrophysiological mechanisms.

Received May 12, 2025;
Accepted October 9, 2025.

Correspondence: lzysyb@126.com

**GRAPHICAL ABSTRACT**

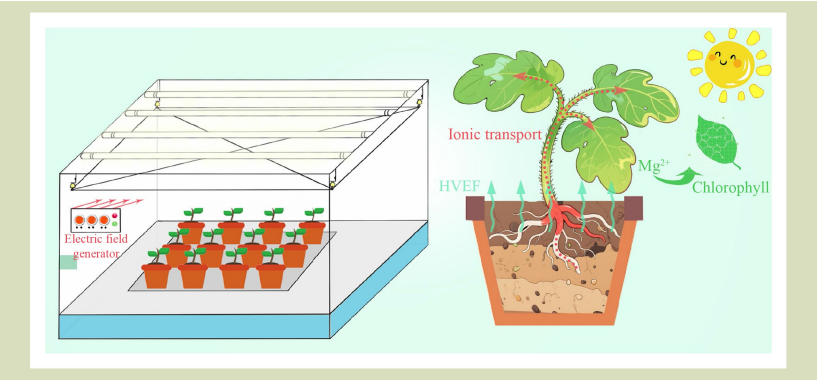


**ABSTRACT**

Tomato is a globally important economic crop whose growth and development are influenced by various environmental factors. As an emerging physical regulation method, high-voltage electrostatic fields (HVEF), has recently gained attention in plant growth modulation. This study investigates the effects of positive (+HVEF) and negative HVEF (−HVEF) on the phenotypic characteristics, microstructure and mechanical properties of tomato seedlings. Fourier-transform infrared spectroscopy, inductively coupled plasma analysis and electrical characterization techniques, were used to systematically examine changes in functional group distribution and ion profiles within plant tissues. The results show that +HVEF treatment for 25 d significantly enhanced the mechanical strength and photosynthetic performance of tomato seedlings. These improvements were associated with the modulation of polar functional groups and magnesium ion distribution, optimizing the electrophysiological responses of the plant. Electrical measurements further demonstrated that

+HVEF altered membrane potentials and ion channel activities, thereby impacting overall physiologic functions and enhanced membrane hyperpolarization, stimulated key photosynthetic enzyme activities and promoted biomass accumulation in tomato seedlings. This study, through a multiscale analysis, elucidates the synergistic regulation of plant electrophysiology and photosynthesis under electric field exposure. These findings provide a theoretical foundation for the application of electric field technologies in agriculture and offer a basis for integrating equivalent circuit models with plant sensors.



## 1 Introduction

The growing global population and intensifying climate change pose significant challenges to food security[1,2], necessitating innovative agricultural strategies to enhance crop yield and resilience. Current agricultural practices generally rely on chemical fertilizers and genetic modification, which can lead to environmental degradation and long-term sustainability concerns[3,4]. However, research on low-cost, environmentally friendly physical methods for promoting plant growth remains limited. Of these approaches, high-voltage electrostatic field (HVEF) has emerged as a promising alternative to enhance plant growth and development. By regulating biological processes at the cellular and molecular levels, these signals offer a sustainable means to improve crop productivity across diverse environmental conditions[5].

HVEF refers to a stable electric field generated by high voltage, which influences matter or biological systems through electrostatic forces without involving current flow. It has been widely used to regulate cellular growth, metabolism and material transport. Plants inherently possess bioelectrical properties, where the distribution of ions across the cell membrane, cytoplasm and intercellular spaces forms a complex electrophysiological system[6–9]. The application of an external electric field can alter membrane potential, ion flux, cell wall structure, photosynthesis and antioxidant systems, significantly affecting plant growth. HVEF has been shown to enhance seed hydrophilicity, influence seed viability, and promote wheat seed germination. Presowing treatment with HVEF can improve seed stability and disease resistance[10]. In tomatoes, HVEF has been reported to extend shelf life by reducing microbial growth and modulating enzyme activity[11]. However, despite these advantages, the effects of HVEF remain highly dependent on field strength, frequency and exposure duration[12–14]. The underlying mechanisms governing plant responses to electrical signals of different polarities remain insufficiently understood, including the biphasic regulatory effect of HVEF on plant growth, time-dependent responses and electrophysiological interactions. A systematic investigation into the interaction between HVEF and plant physiological characteristics is essential for optimizing its application in agriculture[15].

The dynamic distribution and transmembrane transport of ions are fundamental to plant physiological metabolism[16]. External electric fields can drive ion migration and redistribution through dielectrophoretic and electroosmotic effects, thereby modulating physiological functions. Magnesium ions, as central components of chlorophyll and cofactors for photosynthetic enzymes[17], are critical for photosystem II stability[18,19] and the catalytic activity of RuBisCO in the Calvin cycle[20]. $Mg^{2+}$ accumulation in the chloroplast stroma directly stabilizes photosystem II reaction centers, while fluctuations in cytosolic $Mg^{2+}$ concentrations can influence photophosphorylation efficiency by altering ATP synthase conformation[21]. Directional $Mg^{2+}$ transport in vascular tissues may regulate enzymes involved in lignin biosynthesis, such as phenylalanine ammonia-lyase, thereby enhancing mechanical support. In mesophyll cells, subcellular $Mg^{2+}$ compartmentalization, particularly targeted transport to chloroplast membranes, can improve light energy capture and electron transport chain coordination. Additionally, electric fields can modulate $Mg^{2+}$ transporter activity (e.g., the CorA family)[22] through electrostatic interactions, disrupting ion homeostasis and activating intracellular signaling cascades, such as calcium signaling networks. These processes may lead to epigenetic modifications and metabolic reprogramming,

ultimately reshaping photosynthetic pathways. Thus, the regulation of photosynthesis by HVEF involves a cascade of processes linking ion spatial redistribution, metabolic flux realignment and energy conversion efficiency. Changes in plasma membrane potential and the associated electrical signals play a central role in regulating photosynthesis. Sukhova et al.[23] demonstrated that action potentials and variation potentials in plants can suppress $H^+$-ATPase activity, leading to extracellular alkalization, which inhibits mesophyll $CO_2$ diffusion and rapidly alters photosynthetic rates. Building on this, Kozlova et al.[24] introduced the concept of the plant electrome, highlighting how hyperpolarization signals can coordinately modulate stomatal conductance, mesophyll conductance and photosystem II photochemical efficiency to achieve fine-tuned control of carbon fixation. Thus, plant electrophysiological activity through shifts in membrane potential and ion channel activation regulates chlorophyll-dependent light capture, carbon assimilation, and the activity of photosynthetic enzymes. Exogenous electric fields similarly impose transmembrane potential gradients and modulate ion fluxes. For example, tomato seedlings exposed to high-voltage electrostatic fields (2.3–2.5 $kV \cdot cm^{-1}$) show enhanced uptake of $NH_4^+$ and $NO_3^-$ and activation of multiple membrane channels. However, most existing studies have focused on the macroscopic effects of electric fields on plant morphology or growth rates, while the spatiotemporal dynamics of ion migration and their mechanistic links to photosynthetic function remain insufficiently explored.

In this study, we investigated the effects of HVEF on the growth and development of tomato plants. The research focused on phenotypic traits, microstructural tissue organization, mechanical properties and electrophysiological responses. Specifically, we examined how HVEF exposure modulates the expression of functional groups, the spatial distribution of ions, particularly $Mg^{2+}$, and ion transport dynamics across cellular membranes. Our results revealed a potential mechanism by which electric field stimulation influences photosynthetic processes through the regulation of membrane potential, charge redistribution and ion fluxes. By integrating physiological observations with dielectric and mechanical analyses, this study provides mechanistic insight into how external electrostatic fields reshape plant structure and function at multiple biological scales. The findings lay a theoretical foundation for integrating equivalent electrical circuit models with sensor networks in controlled plant systems, thereby advancing the field of plant electrophysiology. In addition, our research contributes to the fundamental understanding of plant-electric field interactions and offers promising avenues for applying electrostimulation technologies in precision agriculture and sustainable crop management.

## 2 Materials and methods

### 2.1 Experimental method

This experiment used a soilless cultivation system to grow tomato seedlings. Before sowing, damaged seeds were removed and the remaining seeds were soaked in clean water for 1–2 h, followed by stirring in 55 °C warm water for 5–10 min and subsequent immersion for 3–4 h. The seeds were then treated with a 0.07% methyl thiophanate for 5–10 min, rinsed with sterile water 3–5 times, and sown in rectangular nutrient pots (7 cm × 5 cm × 7.3 cm, 260 mL volume) filled with nutrient soil. After thoroughly watering the soil, three 23 cm deep holes were made in each pot, with two tomato seeds placed in each hole, followed by soil coverage. Twelve pots were placed in each plastic tray, with the water level maintained at about1 cm. Tomato seeds were initially germinated on trays covered with plastic film and maintained in a climate-controlled chamber at 28 °C with 40% relative humidity for 5–8 h. Subsequently, seedlings were cultivated under 27 °C daytime temperature (11 h of light), 17 °C nighttime temperature (13 h of darkness), 40% relative humidity and a light intensity of 1700 $\mu mol \cdot m^{-2} \cdot s^{-1}$ until seedling emergence.

Once the seedlings emerged, the plastic film was removed, and those with uniform height and growth were selected. The seedlings were divided into three groups and placed in high-voltage electrostatic cultivation chambers under different electric field treatments (Fig. 1): a –15 kV negative high-voltage electric field (–HVEF), no electric field (CK), and a 15 kV positive high-voltage electric field ( HVEF). Both +HVEF and –HVEF treatments were applied continuously throughout the day, with temperature control set to 20–25 °C during the day and 12–15 °C at night, while the electric field output voltage was maintained at 15 kV with an output power of 8 W.

### 2.2 Phenotypic characteristics

Plant growth was evaluated using Dimigizer software (precision = 0.001 $cm^2$) to measure plant height and root

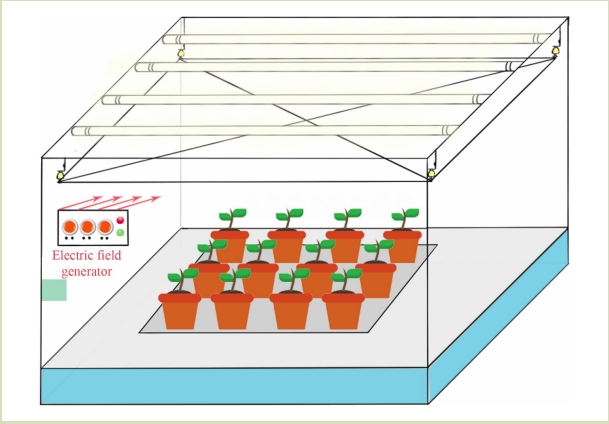


**Fig. 1** Schematic diagram of the application of an electric field to tomato plants.

length. Tensile and compression tests on 25-d-old tomato stems were conducted with a 5544 universal testing machine (Instron, Norwood, MA, USA). For each experimental replicate, three tomato seedlings were randomly selected and measured three times per plant. Microscopic structural observations of stem and leaf tissues were performed using a DM6B fluorescence microscope (Leica, Wetzlar, Germany) following paraffin section staining.

The microstructure of tomato tissues was further examined with a scanning electron microscope (SEM; JSM-IT500HR, JEOL, Japan). Roots, stems and leaves were washed with deionized water and fixed in 2.5% glutaraldehyde for 4 h. Samples were dehydrated through an ethanol gradient (30%, 50%, 70%, 90% and 100%), dried, and sputter-coated with gold using an ion coater (E1010, Hitachi, Tokyo, Japan).

## 2.3 Ionic composition

The distribution of $Mg^{2+}$ ions in tomato seedling roots, stems and leaves were analyzed using inductively coupled plasma optical emission spectrometry (ICP-OES; PerkinElmer, Shelton, CT, USA). Tomato tissues were thoroughly rinsed with deionized water and dried in an oven at 70 °C. Dried samples (10 mg each) were immersed in 6 mL of a mixed solution of nitric acid and hydrogen peroxide (5:1, v/v) for 10 h. The digested solutions were diluted to a final volume of 50 mL, centrifuged at 5000 $r \cdot min^{-1}$ for 5 min, and the supernatants were further diluted with 1% nitric acid to a concentration of 100 ppm. The $Mg^{2+}$ content in each tissue was then determined by ICP-OES. Three tomato seedlings were randomly selected and measured three times per plant.

## 2.4 Electrochemical characterization

The electrochemical impedance spectra of tomato seedling roots, stems and leaves were measured using a CHI660E electrochemical workstation (CH Instruments, Bee Cave, TX, USA) in 0.5 $mol \cdot L^{-1}$ $Na_2SO_4$ solution. A conventional three-electrode system was employed, consisting of a platinum plate (1.0 $cm^2$) as the counter electrode, a standard Ag/AgCl electrode as the reference electrode, and a working electrode prepared by depositing a composite Nafion solution (5%) onto an fluorine-doped tin oxide substrate (1.0 $cm^2$).

The membrane potential was measured by recording the voltage difference between a glass microelectrode (L/M-3P-A; List-Medical, Germany) filled with 3 $mol \cdot L^{-1}$ KCl inserted into the cell and a reference electrode (Ag/AgCl) immersed in the bathing medium.

## 2.5 Biomass characterization

We selected three tomato seedlings with similar sizes on day 25 under the three electric field treatments to measure biomass accumulation. The seedlings were rinsed with deionized water and separated into leaves, stems and roots. Samples were first heated at 105 °C for 30 min for rapid enzyme deactivation, followed by drying at 80 °C for 48 h before weighing. These procedures were applied to determine biomass under different electric field treatments on day 25.

## 2.6 Photosynthesis characterization

Tomato seedlings at various growth stages were exposed to functional electrostatic field treatments. For photosynthetic parameter measurements, healthy leaves (the first leaf) were selected. Net photosynthetic rate, intercellular $CO_2$ concentration and stomatal conductance were determined using a portable photosynthesis system (LI-COR, Lincoln, NE, USA) under controlled greenhouse conditions maintained at 25 ± 1 °C and 60%–70% relative humidity. Three leaves per plant were measured, with three biological replicates per treatment.

For stomatal observation, fully expanded functional leaves (the second to third true leaves from the apex downward) were selected for measurements at 9:00 am. After rinsing with distilled water to remove dust, epidermal peels were manually obtained using forceps, mounted on glass slides and examined under an optical microscope (400×). Stomatal aperture status was quantified through direct counting.

The activities of key photosynthetic enzymes in tomato leaves, including ribulose-1,5-bisphosphate carboxylase/oxygenase (rubisco), sedoheptulose-1,7-bisphosphatase (SBPase), fructose-1,6-bisphosphate aldolase (FBA), and transketolase (TK), were quantified using assay kits (Shanghai Youxuan Biotechnology Co., Ltd., Shanghai, China). Three tomato seedlings were randomly selected and measured three times per plant.

Chlorophyll content was measured following the methods: fully expanded leaves were air-dried at room temperature, and 1 g of leaf tissue was arbitrarily sampled and incubated in 100% acetone for 12 h in the dark until complete decolorization. The absorbance of the extract was measured at 665 nm (chlorophyll a) and 649 nm (chlorophyll b) using a UV-Vis spectrophotometer. Each experiment was performed in triplicate. Total chlorophyll content was calculated using the formula:

$$\text{Total chlorophyll} = \text{chlorophyll a} + \text{chlorophyll b} \quad (1)$$

$$\text{Chlorophyll a (mg/L)} = 13.70 \times A_{665} - 5.76 \times A_{649} \quad (2)$$

$$\text{Chlorophyll b (mg/L)} = 25.80 \times A_{649} - 7.60 \times A_{665} \quad (3)$$

### 2.7 Data analysis

Data processing and analysis were performed using Microsoft 365 for data collection and organization. Statistical analyses including correlation analysis and significance testing between treatments were conducted using SPSS 26 with the least significant difference method at $\alpha = 0.05$.

## 3 Results and discussion

### 3.1 Phenotypic characteristics and dielectric properties

Tomato seedlings were exposed to different HVEF and measured every 5 d after being placed in the electric field. In the +HVEF group, the first true leaf emerged on day 6, while neither the −HVEF nor CK group had leaf development. On day 7, the −HVEF group produced true leaves, whereas the CK group remained unchanged. By day nine, the CK group had also developed true leaves. As shown in Fig. 2, plant traits were assessed from day 15 onward. Before day 25, HVEF promoted all measured growth parameters, with the +HVEF group

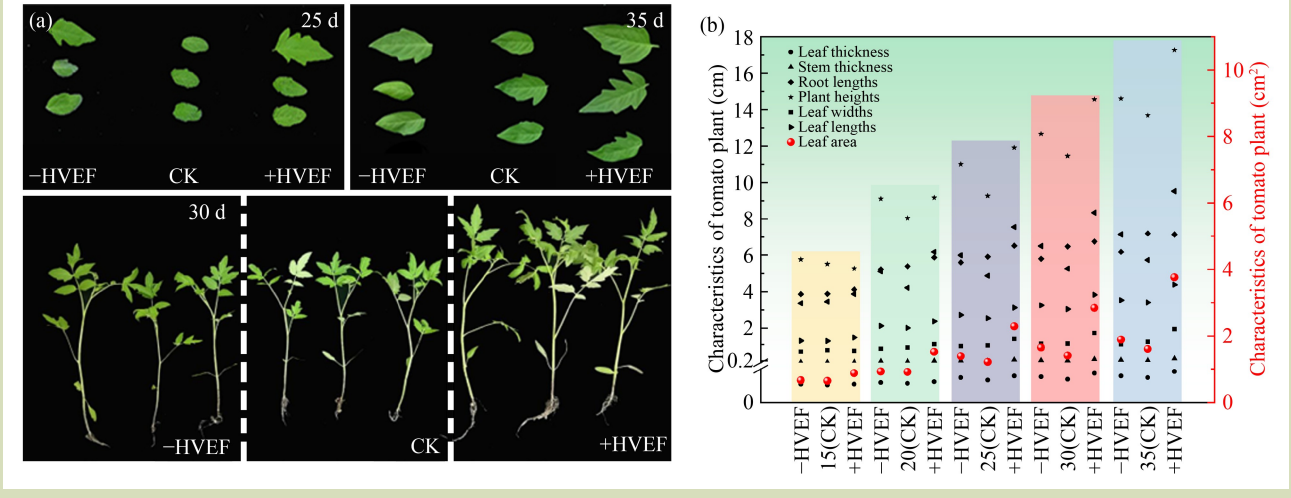


**Fig. 2** (a) Phenotypic presentation and (b) phenotypic data of tomato seedlings under different electric field treatments. −HVEF, negative high-voltage electric field; CK, no electric field; and +HVEF, positive high-voltage electric field.

exhibiting a higher growth rate than the −HVEF group. However, after day 25, growth in the −HVEF group was inhibited[25,26].

Based on growth indicators, positive and negative electric fields had distinct effects on tomato seedling development. +HVEF gave a continuous and enhanced promotive effect. From day 15, the number of leaves increased significantly ($p < 0.05$), with further enhancement by day 35 ($p < 0.01$). Stem diameter was significantly increased on day 25 ($p < 0.05$) and day 35 ($p < 0.01$). Leaf area expanded significantly on day 20 ($p < 0.05$), day 30 ($p < 0.01$) and day 35 ($p < 0.01$). Leaf length also increased significantly on days 30 and 35 (both $p < 0.01$). The increasing levels of statistical significance over time (from $p < 0.05$ to $p < 0.01$) indicate a cumulative effect under +HVEF. In contrast, −HVEF initially promoted growth, but the effect diminished over time. From days 15 to 25, the number of leaves increased significantly (15 d, $p < 0.05$; 20 d, $p < 0.05$; 25 d, $p < 0.01$). A transient increase in leaf area was observed on day 30 ($p < 0.05$). However, from days 30–35, the promotive effect weakened, with no significant differences observed in leaf number, stem diameter, leaf length or leaf area ($p > 0.05$).

As shown in Fig. 3, the biomass of tomato seedlings differed significantly under the three electric field treatments. The highest biomass was observed under +HVEF treatment. This can be attributed to the stimulation of root cell membrane hyperpolarization by +HVEF, which activates ion channels and enhances the absorption of $Mg^{2+}$ and other nutrients. Additionally, the net photosynthetic rate increased, leading to higher Calvin cycle flux and enhanced carbon fixation, thus promoting biomass accumulation[27,28]. Notably, the difference in leaf biomass was the most significant among all plant organs, likely due to the central role of leaves in photosynthesis.

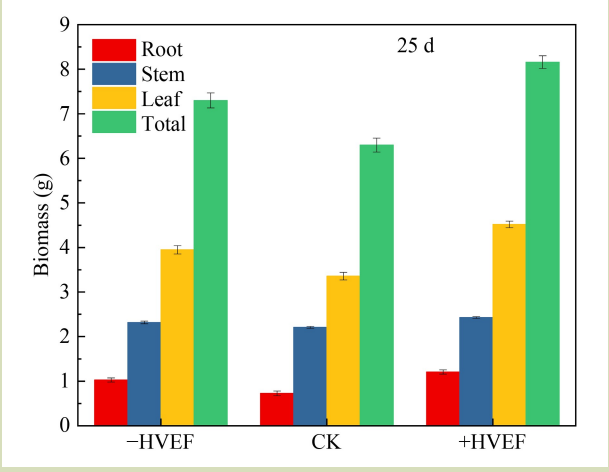


**Fig. 3** Biomass of tomato seedlings 25 d after being placed under three electric field treatments: −HVEF, negative high-voltage electric field; CK, no electric field; and +HVEF, positive high-voltage electric field. Means with the same letters are not significantly different ($p > 0.05$) between treatments for the same plant material.

Impedance measurements were conducted on tomato seedlings at different growth stages under the three treatments: −HVEF, CK and +HVEF. As shown in Fig. 4(a–c), leaf impedance increased steadily in both the CK and +HVEF groups, whereas the −HVEF group had an initial increase followed by a decrease. In the CK environment, leaf membrane potential remained stable, with normal metabolic regulation closing ion channels, reducing ion leakage, and thereby increasing impedance. The +HVEF condition facilitated cation accumulation inside cells, suppressing cation channel activity and further reducing ion mobility, leading to a continuous rise in impedance. In contrast, −HVEF-induced membrane depolarization, activating ion channels and triggering a transient ion influx. However, cells rapidly adjusted to restore membrane resistance, resulting in an initial impedance increase followed by a decrease[29,30]. As shown in Fig. 4(d), root impedance in the −HVEF group initially decreased before day 15 and then increased. This trend was attributed to −HVEF-induced membrane depolarization, which activated anion channels and enhanced proton pump activity to maintain ion gradients, thereby increasing conductivity and lowering impedance. Additionally, root cells likely responded to the electric field by actively absorbing nutrient ions, increasing transmembrane currents. However, prolonged exposure to −HVEF triggered an adaptive repair mechanism to mitigate oxidative membrane damage, restoring membrane integrity and leading to a subsequent impedance increase[31,32]. In the +HVEF group, root impedance continuously decreased until day 35, after which it began to rise Fig. 4(e). This decrease resulted from cation accumulation in root tissues, forming a localized high-concentration barrier that inhibited essential ion uptake through ion channels, leading to intracellular ion depletion. As a compensatory response, ion channels opened, increasing membrane conductivity and further reducing impedance. After day 35, hormonal regulation facilitated resource redistribution, prioritizing membrane repair or osmolyte synthesis, partially restoring membrane resistance

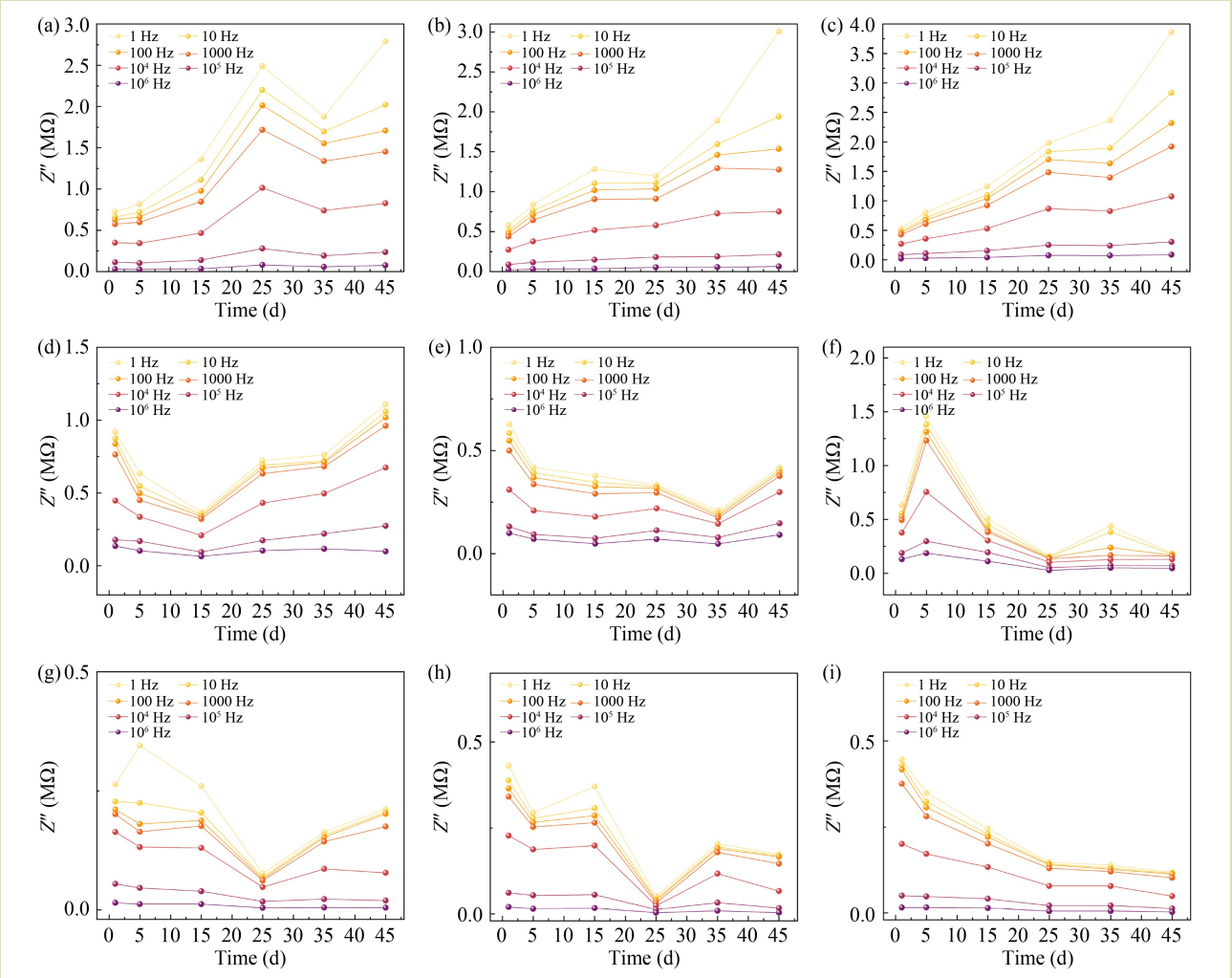


**Fig. 4** Impedance of tomato leaves in (a) a negative high-voltage electric field (−HVEF); (b) no electric field; and (c) a positive high-voltage electric field (+HVEF); roots in (d) −HVEF, (e) +HVEF and (f) CK; and stems in (g) −HVEF, (h) CK and (i) +HVEF.

and increasing impedance. In the CK group, root impedance peaked on day 5 (Fig. 4(f)). Without external electric field interference, initial ion uptake relied on passive diffusion, resulting in low membrane channel activity and high impedance. As growth metabolism intensified, active ion transport increased, leading to a gradual impedance decline. Figure 4(g) shows that stem impedance in the −HVEF group first decreased due to membrane depolarization and ion channel activation but later increased due to adaptive repair mechanisms. In the CK group, impedance initially decreased and then increased during normal stem growth (Fig. 4(h)). In the +HVEF group, sustained membrane depolarization and ion channel regulation led to a continuous impedance decline (Fig. 4(i)[33].

Overall, Fig. 4 illustrates that root and stem impedance followed the trend CK > −HVEF > +HVEF. In the low-frequency range, −HVEF primarily suppressed ion flow, resulting in lower conductivity. As frequency increased, this inhibitory effect weakened, gradually enhancing conductivity. Meanwhile, +HVEF facilitated ion flow, leading to lower impedance. Leaf impedance remained relatively consistent across the three electric field treatments, primarily influenced by photosynthesis. Frequency also affected the capacitive

properties of cell membranes. At low frequencies, impedance was primarily resistance-dominated, whereas at high frequencies, capacitance became the dominant factor. As frequency increased, plant impedance generally decreased due to enhanced ion mobility and electrical conductivity, ultimately reducing impedance[34,35].

Membrane hyperpolarization is considered an initiative step for stomatal opening. As shown in Table 1, both mesophyll and guard cell membrane potentials had a progressive hyperpolarization trend over the growth period (5, 15, 25 and 35 d). This indicates that HVEF significantly enhances the hyperpolarization of cell membranes, potentially promoting $H^+$ efflux and $K^+$ influx, thereby increasing stomatal pores and elevating stomatal conductance[36]. The resulting increase in conductance facilitates $CO_2$ uptake into the leaf, contributing to enhanced photosynthetic rates. Specifically, +HVEF appears to moderately hyperpolarize the membrane, which may activate $H^+$-ATPases and $K^+$ channels[37], enabling optimal stomatal opening and improved $CO_2$ assimilation in mesophyll cells. In contrast, prolonged exposure to −HVEF may induce excessive hyperpolarization of guard cell membranes[38]. This could result in uncontrolled $K^+$ influx, loss of turgor balance, and impaired stomatal[39], ultimately restricting $CO_2$ diffusion and reducing photosynthetic efficiency. These physiologic disruptions likely explain the growth inhibition observed after 25 d in the −HVEF group[39,40]. In the CK group, membrane potential remained relatively stable, fluctuating around −90 mV in both mesophyll and guard cells.

Figure 5(a–c) presents the Bode plots of 25 d tomato roots, stems and leaves under −HVEF, CK, and +HVEF. As the current frequency increased, the phase angle initially rose and then declined, reaching its maximum near $10^5$ Hz. According to the equation $fc = 1 / (2\pi \times Rm \times Cm)$, where fc is the frequency at the phase angle peak, Rm denotes membrane resistance, and Cm is membrane capacitance, the phase angle peak in the +HVEF group shifted toward higher frequencies compared to the CK group. This shift was due to the lower Rm in the +HVEF condition, where the electric field drove cations to accumulate on the extracellular membrane surface, causing membrane hyperpolarization. This induced tighter lipid packing, increasing membrane thickness or reducing membrane area, thereby decreasing Cm. Conversely, phase angle peak of the the −HVEF group shifted toward lower frequencies, as −HVEF increased Rm and induced membrane depolarization, leading to a more disordered lipid arrangement or membrane expansion, which increased Cm[41,42].

Figure 5(d–f) shows the Nyquist plots of 25 d tomato roots, stems and leaves. Each tissue had two semicircular arcs in the impedance spectra. The low-frequency semicircle corresponded to cell membrane interfacial polarization, reflecting the combined effect of Rm and Cm, which was associated with ion channel activity. The high-frequency semicircle primarily reflected cytoplasmic and cell wall resistance, linked to ion migration within the cell wall[43]. The Nyquist plots revealed that the arc radius under +HVEF was smaller than those under −HVEF and CK, indicating enhanced conductivity and increased charge transfer rates in plant tissues under +HVEF treatment. Equivalent circuit modeling using ZSimpWin software further elucidated the effects of electric field treatments on plant tissues (Table 2). The equivalent circuit model for tomato roots was R(Q(R(QR))), with an iteration count of 4 and a chi-square value of 0.00244 (where R represents a resistor, Q represents a constant phase element,

**Table 1 Membrane potential of tomato seedlings at four cultivation days under three electric field treatments**

| Cell | Cultivation time (d) | −HVEF (mv) | CK (mv) | +HVEF (mv) |
|---|---|---|---|---|
| Mesophyll cell | 5 | −106 ± 6.2 | −91.6 ± 6.9 | −94.3 ± 5.1 |
| | 15 | −120 ± 5.6 | −86.2 ± 6.1 | −101 ± 4.3 |
| | 25 | −129 ± 4.4 | −82.8 ± 5.1 | −104 ± 3.2 |
| | 35 | −124 ± 5.4 | −86.9 ± 6.2 | −105 ± 4.6 |
| Guard cell | 5 | −127 ± 5.8 | −102 ± 6.8 | −109 ± 6.1 |
| | 15 | −142 ± 5.2 | −94.2 ± 5.3 | −114 ± 5.3 |
| | 25 | −149 ± 5.8 | −91.2 ± 4.8 | −125 ± 4.5 |
| | 35 | −148 ± 5.4 | −90.6 ± 5.7 | −125 ± 5.1 |

Note: −HVEF, negative high-voltage electric field; CK, no electric field; and +HVEF, positive high-voltage electric field.

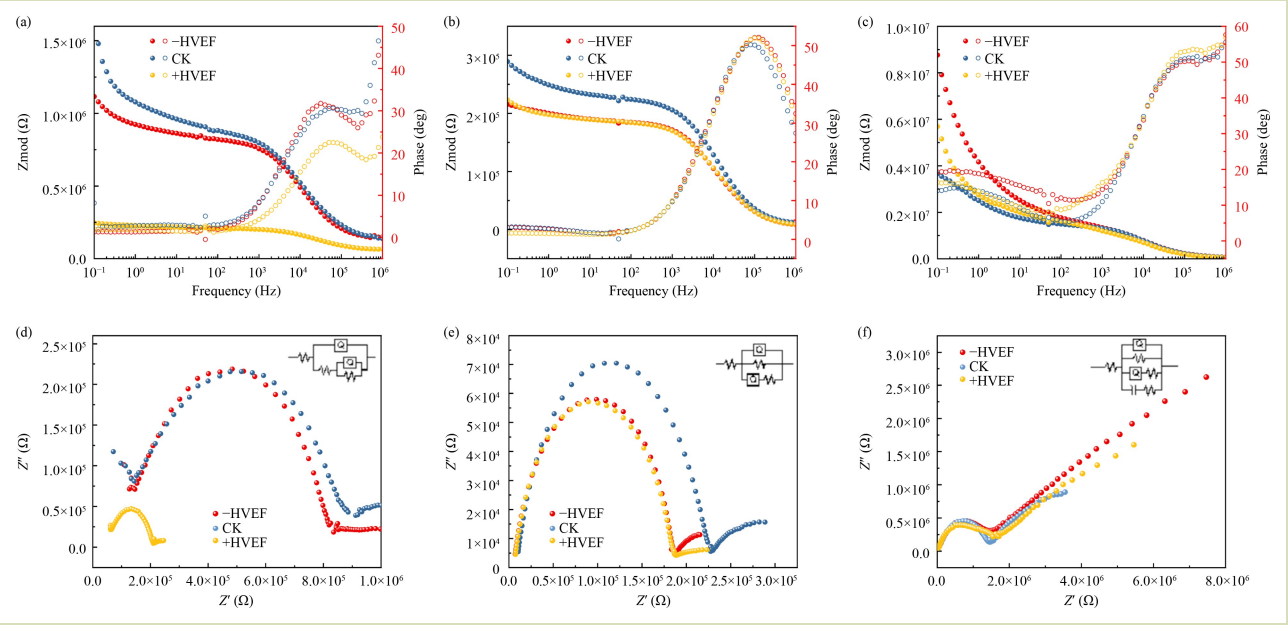


**Fig. 5** Bode plots of tomato (a) roots, (b) stems and (c) leaves; and Nyquist plots of (d) roots, (e) stems, and (f) leaves. − HVEF, negative high-voltage electric field; CK, no electric field; and + HVEF, positive high-voltage electric field.

**Table 2 Fitted values of parameters of equivalent circuit model for tomato plants**

| Physical parameter | −HVEF | | | CK | | | +HVEF | | |
|---|---|---|---|---|---|---|---|---|---|
| | Root | Stem | Leaves | Root | Stem | Leaves | Root | Stem | Leaves |
| R (Ω·cm$^2$) | 4.318E+04 | 3.608E+03 | 8.080E+03 | 5.271E+04 | 6.674E+03 | 2.264E+03 | 4.148E+04 | 2.877E+03 | 1.566E+05 |
| CPE1 (S-sec$^n$·cm$^{-2}$) | 7.470E-09 | 1.420E-09 | 5.676E-10 | 7.965E-09 | 2.095E-09 | 5.023E-10 | 4.592E-09 | 2.452E-09 | 4.264E-10 |
| $n1$ ($0<n<1$) | 5.904E-01 | 7.840E-01 | 6.698E-01 | 6.291E-01 | 7.573E-01 | 6.585E-01 | 6.38E-01 | 7.791E-01 | 6.612E-01 |
| R1 (Ω·cm$^2$) | 7.052E+05 | 2.737E+05 | 1.892E+07 | 7.365E+05 | 2.734E+05 | 1.365E+07 | 3.15E+05 | 1.705E+05 | 2.822E+10 |
| CPE2 (S-sec$^n$·cm$^{-2}$) | 7.558E-05 | 5.729E-08 | 1.331E-07 | 6.327E-06 | 2.603E-06 | 1.393E-07 | 1.029E-05 | 4.415E-07 | 1.160E-07 |
| $n2$ ($0<n<1$) | 6.903E-01 | 5.937E-01 | 3.666E-01 | 7.153E-01 | 6.960E-01 | 4.816E-01 | 7.423E-01 | 6.700E-01 | 4.199E-01 |
| R2 (Ω·cm$^2$) | 3.734E+05 | 9.431E+05 | 1.980E+06 | 4.034E+05 | 1.473E+06 | 2.393E+06 | 3.164E+05 | 4.812E+05 | 2.411E+06 |
| C (F·cm$^{-2}$) | | | 1.863E-12 | | | 9.970E-09 | | | 8.770E-13 |
| R3 (Ω·cm$^2$) | | | 6.810E+05 | | | 2.333E+06 | | | 8.134E+06 |

Note: −HVEF, negative high-voltage electric field; CK, no electric field; and +HVEF, positive high-voltage electric field.

and the parentheses denote the configuration of these components). For stems, the model was R(QR(QR)), with six iterations and a chi-square value of 0.0000454. The leaf model was R(QR(QR)(CR)), with three iterations and a chi-square value of 0.000117. These models provided deeper insights into the regulatory mechanisms of electric field treatments on plant tissues[41].

## 3.2 Micromorphology and ionic composition

Microscopic morphology of 25 d tomato seedlings under the three electric field treatments was analyzed using SEM. As shown in the leaf SEM images (Fig. 6(a)), +HVEF treatment significantly increased stomatal density and aperture size. Stomata were more densely and uniformly distributed with clearer structures, indicating enhanced stomatal conductance

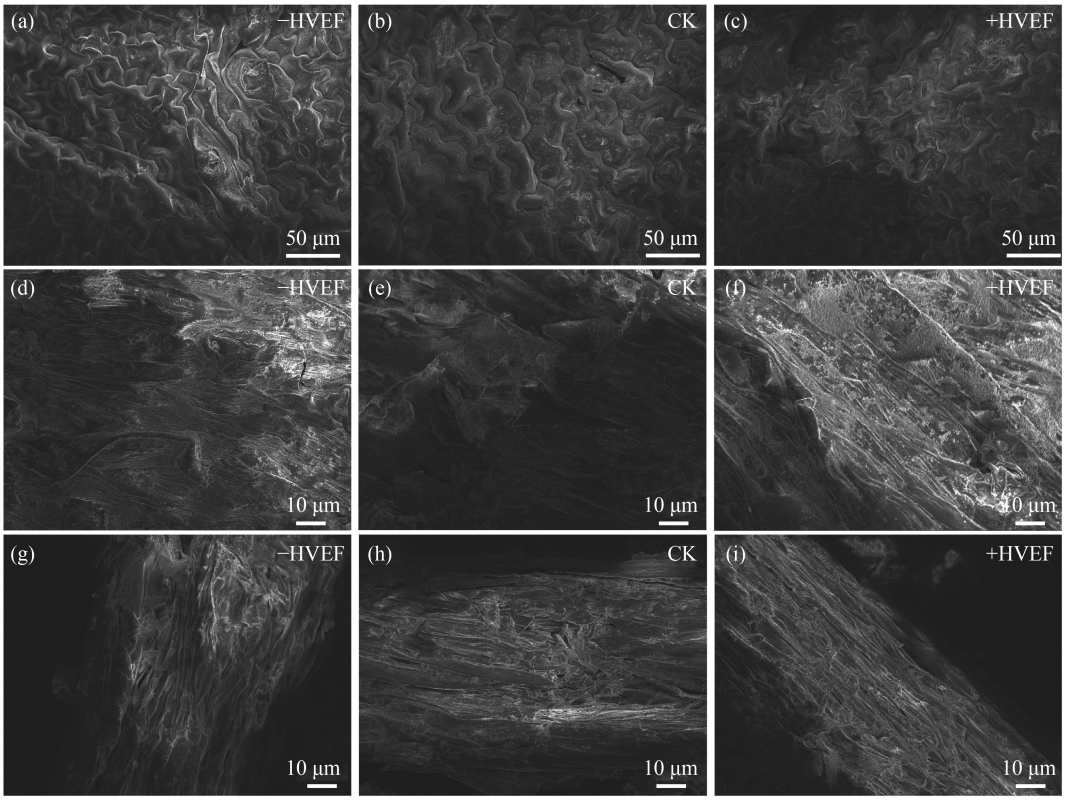


**Fig. 6** Scanning electron micrographs of tomato seedlings under three electric field treatments: (a), (b) and (c) leaf, (d), (e) and (f) stem and (g), (h) and (i) root. −HVEF, negative high-voltage electric field; CK, no electric field; and +HVEF, positive high-voltage electric field.

and photosynthetic activity. In the CK group, stomata had normal opening, while in the −HVEF group, stomatal opening was intermediate between CK and +HVEF but had a disorganized distribution, potentially disrupting gas exchange. SEM images of the stems (Fig. 6(b)) revealed that +HVEF promoted thickening and expansion of the vessel walls, which likely enhanced ion transport and increased stem mechanical strength. Root SEM images (Fig. 6(c)) showed that +HVEF treatment resulted in greater root hair density and length compared to CK and −HVEF groups, facilitating improved ion absorption from the soil and promoting overall plant growth and development[44].

Energy dispersive spectroscopy mapping was used to analyze the distribution of ions in the leaves, stems and roots of tomato seedlings after 25 d under +HVEF treatment. In Fig. 7(a), $K^+$ is evenly distributed in the leaves, indicating that the electric field promotes the entry of $K^+$ into guard cells, helping maintain stomatal opening and enhancing transpiration and photosynthetic efficiency. High concentrations of $Ca^{2+}$ and $Mg^{2+}$ are also present. $Ca^{2+}$ stabilizes membrane structures, while $Mg^{2+}$, as the central ion of chlorophyll, enhances photosynthesis. The uniform distribution of O and C indicates active metabolic activity and vigorous organic matter synthesis in the leaves. In Fig. 7(b), the accumulation of $Ca^{2+}$ enhances the stability of calcium bridges in the cell wall, increasing mechanical strength and conductivity. The distributions of $K^+$ and $Mg^{2+}$ are also well-organized: $K^+$ regulates osmotic pressure and pressure conduction, and $Mg^{2+}$ may be involved in ATPase reactions[17]. In Fig. 7(c), both $K^+$ and $Ca^{2+}$ are highly concentrated, particularly in the root hair region, indicating that the electric field promotes active nutrient ion absorption by the roots. The uniform distribution of $Mg^{2+}$ further supports root metabolism.

Fourier-transform infrared spectroscopy was used to

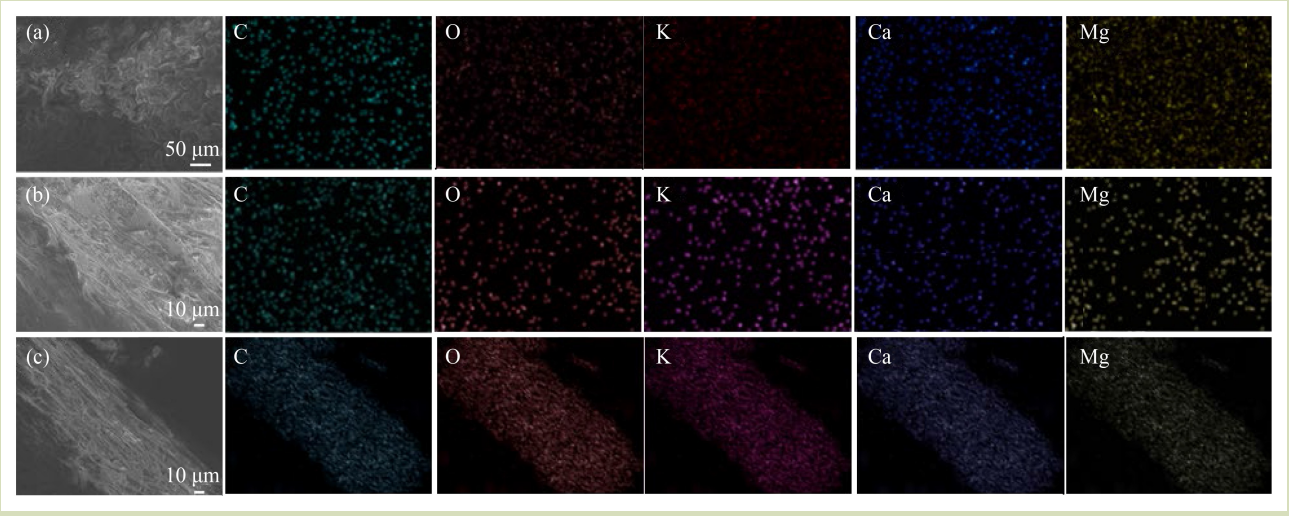


**Fig. 7** Energy dispersive spectroscopy mapping images of tomato seedlings for carbon, oxygen, potassium, calcium and magnesium under a positive high-voltage electric field: (a) leaf, (b) stem and (c) root.

characterize the roots, stems and leaves of tomato seedlings treated with +HVEF for 25 d and to analyze the possible functional groups present. In Fig. 8(a), the absorption peak around 3415 $cm^{-1}$ corresponds to the stretching vibration of –OH, while the peak at 1065 $cm^{-1}$ corresponds to the stretching vibration of C–O–C, likely originating from cellulose and hemicellulose. The peak around 2929 $cm^{-1}$ corresponds to the stretching vibration of C–H, likely from fatty acids in cell membranes, phytol chains in chlorophyll, and methoxy groups in lignin. The absorption peak at 1636 $cm^{-1}$ corresponds to the stretching vibration of C=O [44], which is related to the amide I band of proteins. The peak at 1430 $cm^{-1}$ corresponds to the vibration of O-$CH_3$, originating from the methoxy-substituted phenyl group in lignin. A broad peak around 500–600 $cm^{-1}$ (metal-oxygen bond) corresponds to the stretching and bending vibrations of metal ions[45], including $Mg^{2+}$, $Ca^{2+}$, and $K^{2+}$, which are present in the tomato seedlings. As leaves are the primary organs for photosynthesis

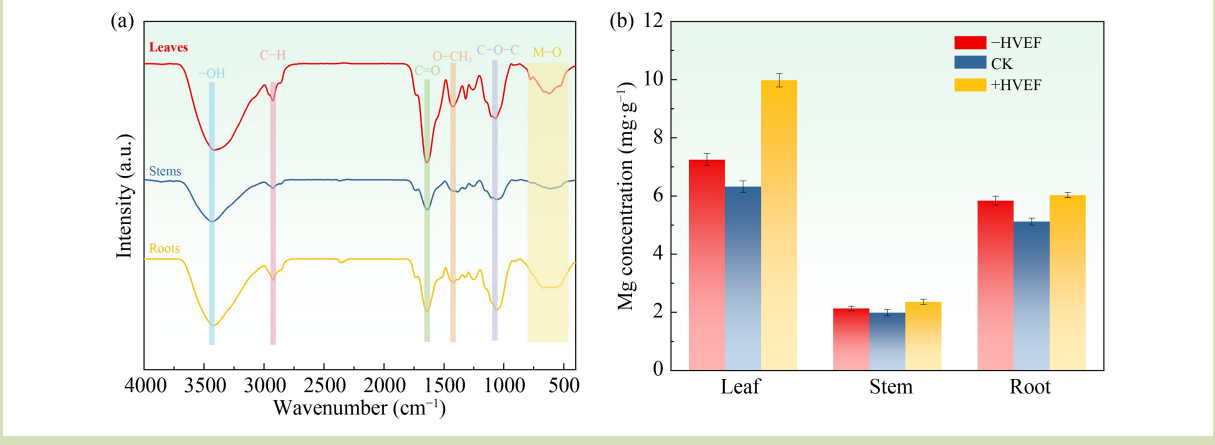


**Fig. 8** (a) Fourier-transform infrared spectroscopy spectrum of tomato seedling tissues, and (b) magnesium content in tomato seedling tissues. –HVEF, negative high-voltage electric field; CK, no electric field; and +HVEF, positive high-voltage electric field.

in tomato seedlings, they are rich in chlorophyll, carotenoids, lipids, and photosynthetic enzymes, which produce strong absorption peaks in the infrared spectrum. The roots exhibit a wider peak in the 500–600 $cm^{-1}$ range due to the diversity of minerals absorbed from the soil[46]. Additionally, the roots store large amounts of starch and soluble sugars, which also result in strong infrared responses. The stems, primarily involved in providing mechanical support and ion transport, show weaker spectral signals.

$Mg^{2+}$ is a key element in chlorophyll, which plays a crucial role in photosynthesis. ICP analysis was conducted to examine the distribution of $Mg^{2+}$ in the leaves under different electric field treatments[47]. Figure 8(b) shows that after 25 d of +HVEF and −HVEF treatment, the $Mg^{2+}$ content in the tomato seedlings significantly increased, particularly in the leaves, where it reached 9.98 $mg·g^{-1}$, 1.38 times higher than the −HVEF group (7.25 $mg·g^{-1}$) and 1.58 times higher than the CK group (6.32 $mg·g^{-1}$). This indicates that the +HVEF treatment facilitates the transport of $Mg^{2+}$ ions into the leaves, increasing their concentration. This process likely involves enhanced charge-driven effects within the plant, promoting the directional movement of $Mg^{2+}$ ions. Additionally, +HVEF treatment improves the ability of the root to absorb ions from the soil, particularly $Mg^{2+}$. The electric field likely affects ion channels in the roots or increases root activity, leading to greater absorption of $Mg^{2+}$, which is then transported to the leaves[48]. Meanwhile, +HVEF enhances $Mg^{2+}$ transport by modulating membrane potential, surface charge distribution, and $Ca^{2+}$ mediated signaling. These changes may facilitate the expression or activity of the AtMRS2/MGT family of $Mg^{2+}$ transporters[49–51]. In parallel, HVEF-induced electric stimulation may promote the opening of cyclic nucleotide-gated channels and activate plasma membrane $H^+$-ATPases[52,53]. The resulting increase in membrane polarization and proton gradient indirectly drives $Mg^{2+}$ absorption and long-distance transport within plant tissues.

### 3.3 Mechanical properties

Elastic modulus is a key indicator of the mechanical properties of tomato stems. As shown in the stress-strain curve (Fig. 9(a)), both +HVEF and −HVEF treatments increased the tensile strength and elastic modulus of tomato stems compared to the CK group. The +HVEF group had a more rapid increase in stress and a higher maximum tensile stress (Fig. 9(c)), indicating that +HVEF promoted cell expansion and cell wall thickening, enhancing resistance to tensile stress. While −HVEF also improved tensile strength, its strain capacity was relatively lower. This may be attributed to its biphasic regulatory effect, where it initially enhances ion transport and growth but later induces an inhibitory effect, increasing cell wall brittleness[54]. In the compression displacement-load curve (Fig. 9(b)), both +HVEF and −HVEF treatments improved compressive strength compared to CK, indicating that the applied electric field enhanced cell wall mechanical properties. The +HVEF-treated stems had greater load-bearing capacity under compression, likely due to the positive electric field facilitating ion transport, accelerating cell division, and promoting cell wall thickening, thereby strengthening structural support. In contrast, the improvement in compressive strength under −HVEF treatment may be linked to its early-stage growth promotion. However, its later inhibitory effects may limit further mechanical enhancement, leading to a smaller increase in strength compared to +HVEF[55].

Figure 10 illustrates the cellular structure of 25 d leaves under −HVEF, CK, and +HVEF treatments. As shown in Fig. 10(a), the leaf cross-section reveals a single-layer epidermis with thin cell walls, well-differentiated palisade and spongy tissues, and the lower epidermis adjacent to loosely arranged spongy cells. Both −HVEF and +HVEF promoted leaf growth, whereas the CK group had normal growth. Leaf cells subjected to external electric field stimulation were noticeably larger, well-organized and clearly distinguishable. Figure 10(b) shows the microscopic structure of tomato stems. The stem cross-section is circular, comprising the epidermis, cortex and vascular cylinder. The epidermal cells are small, with stomata and trichomes. The cortex consists of 5–6 layers of cells, followed by the endodermis, which contains five vascular bundles of varying sizes. The xylem and phloem are clearly defined. In the +HVEF treated group, the epidermal and cambium cells had a more organized structure than those in the −HVEF and CK groups. Additionally, +HVEF treatment resulted in larger, well-arranged cells with an increased cross-sectional area. These structural modifications likely enhanced stem compressive and tensile strength, accelerating plant growth and improving mechanical properties. In contrast, −HVEF treatment led to irregularly sized cells, cortical damage and a loosely arranged cell wall structure, reducing the mechanical integrity of stem tissues. The weakened cell walls compromised stem compressive strength. The observed effects of −HVEF could be attributed to its initial stimulation of ion transport, increased water and nutrient uptake, and enhanced phytohormone

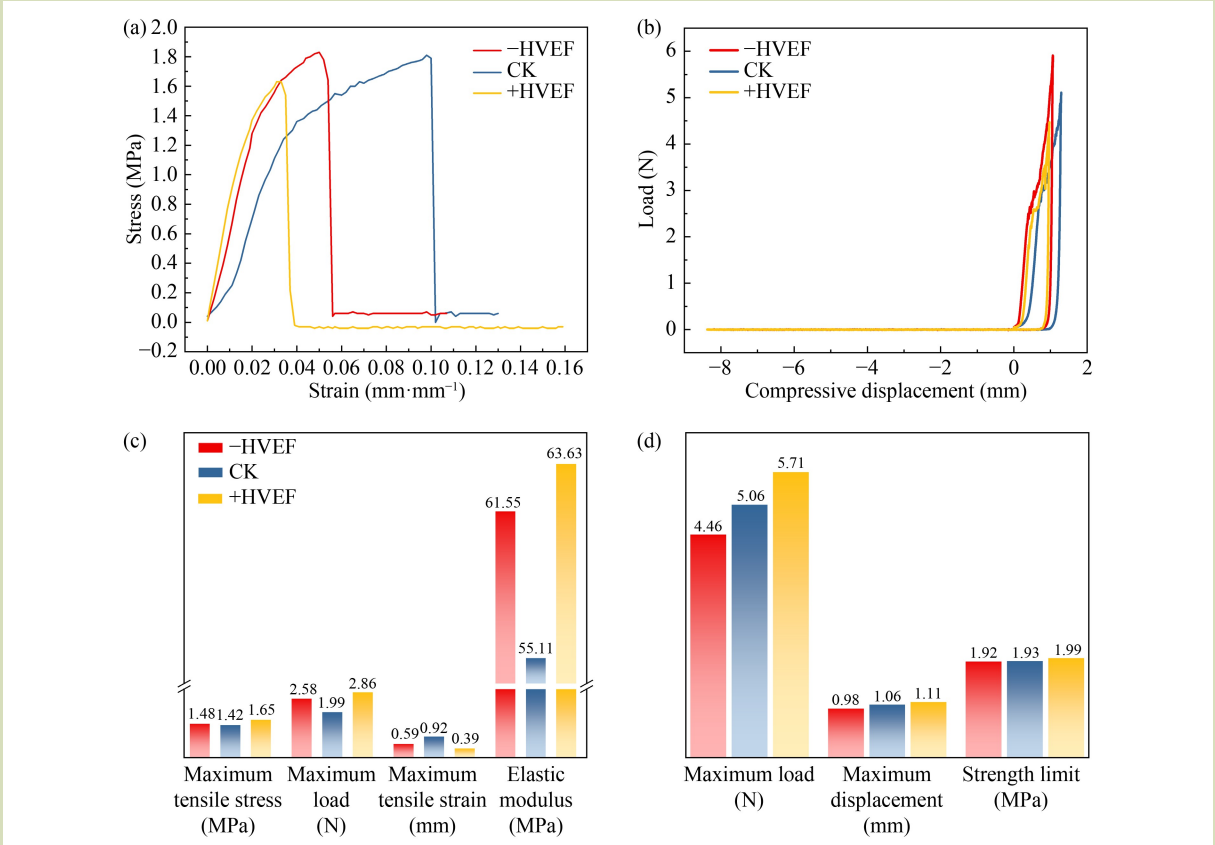


**Fig. 9** (a) Stress-strain curve, (b) compression displacement-load curve, (c) and (d) corresponding data on tensile and compressive strength of tomato seedling tissues. −HVEF, negative high-voltage electric field; CK, no electric field; and +HVEF, positive high-voltage electric field.

secretion, which promoted early-stage growth. However, prolonged exposure to the electric field induced cellular damage, leading to growth inhibition. Positive ions enhance photosynthesis, while negative ions stimulate respiration. During the day, photosynthesis absorbs $CO_2$, whereas at night, respiration releases $CO_2$. Since the treatment was applied continuously, prolonged respiration dominance over photosynthesis resulted in plant weakening and, in severe cases, death. Conversely, when photosynthesis exceeded respiration, organic matter accumulated, promoting plant growth. These findings support the conclusion that +HVEF enhances growth, whereas −HVEF initially stimulates growth but later inhibits it.

## 3.4 Photosynthetic performance

Further microscopic analysis of stomatal morphology under different electric field treatments (Fig. 11) revealed that the +HVEF group had larger, well-defined and more abundant stomata, indicating enhanced stomatal development and opening. In contrast, the CK group had fewer stomata, most of which remained closed, indicating lower stomatal activity in normal conditions. The −HVEF group had an intermediate stomatal density, with some stomata partially open, though less pronounced than in the +HVEF group.

The UV spectrophotometer was used to measure the absorbance of acetone solutions from the leaves of 25-d-old tomato seedlings under the three electric field treatments at wavelengths of 665 and 649 nm to assess chlorophyll content[46]. Figure 12(a) shows that the absorbance of tomato seedlings under +HVEF treatment is significantly higher than that of the −HVEF and control groups. Figure 12(b) shows that the chlorophyll content in the leaves of tomato seedlings under +HVEF treatment was the highest, reaching 14.0 $mg·g^{-1}$. This indicates that +HVEF promotes ion flow, increasing the $Mg^{2+}$

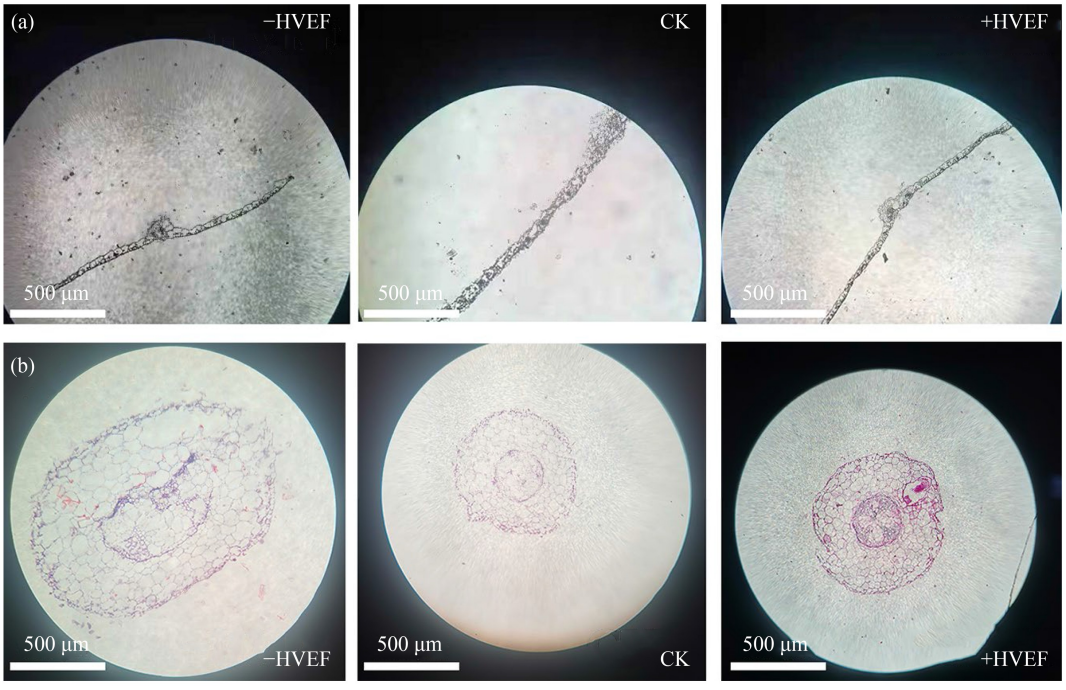


**Fig. 10** Microscopic structure of tomato seedling tissues (a) leaves and (b) stems under three electric field treatments: −HVEF, negative high-voltage electric field; CK, no electric field; and +HVEF, positive high-voltage electric field.

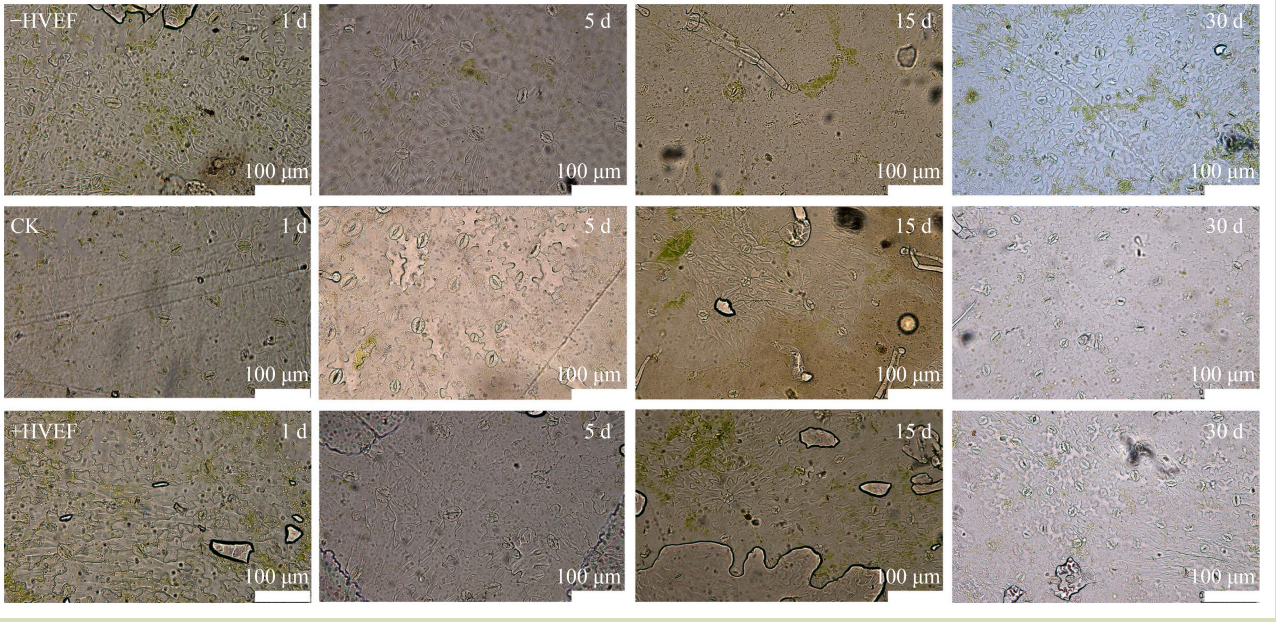


**Fig. 11** Stomatal morphology of tomato seedlings after 1, 5, 15 and 30 d under three electric field treatments: −HVEF, negative high-voltage electric field; CK, no electric field; and + HVEF, positive high-voltage electric field.

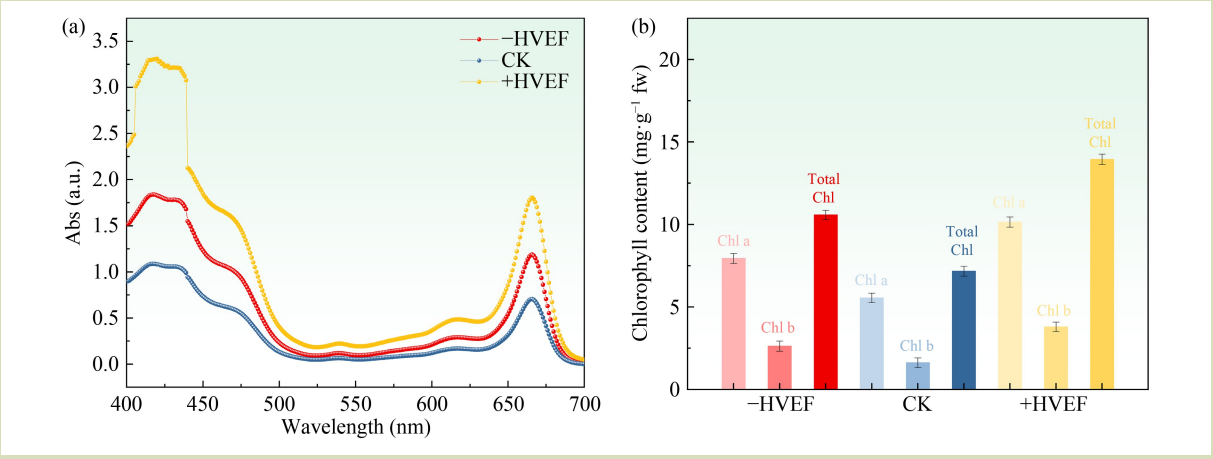


**Fig. 12** (a) Absorbance and (b) chlorophyll (total, Chl a and Chl b) concentration of tomato seedling leaves under three electric field treatments: −HVEF, negative high-voltage electric field; CK, no electric field; and +HVEF, positive high-voltage electric field.

content and enhancing chlorophyll formation, which in turn boosts photosynthesis. Additionally, the electric field increases the mobility of ions, enhancing the metabolic processes in plant tissues. This could improve the activity of enzymes involved in chlorophyll synthesis. The electric field may also improve nutrient absorption from the soil, providing the necessary elements for chlorophyll production. The combined effects of these processes likely contribute to the higher ion content observed[56].

Stomata serve as the primary site for gas exchange and transpiration. In this study, the number of stomata on the abaxial leaf surface was analyzed (Fig. 13(a)). On the first day of exposure to the electric field, the CK group had a significantly higher stomatal density than the +HVEF and −HVEF groups due to the initial stress response. Over time, the stomatal number and growth rate in the +HVEF group increased significantly compared to the −HVEF and CK groups. This trend indicates that the electric field promoted ion channel activity, accelerating cell division and differentiation, ultimately leading to a higher stomatal density. Figure 13(b) illustrates changes in stomatal conductance, the +HVEF treatment significantly enhanced stomatal opening, whereas the −HVEF and CK groups had relatively low values. This effect is attributed to +HVEF-induced changes in the membrane potential of guard cells, facilitating $K^+$ influx, leading to cell expansion and increased stomatal aperture. Stomatal conductance was higher in the morning and gradually decreased in the afternoon, aligning with the diurnal rhythm of stomatal regulation[57,58]. Figure 13(c) presents the photosynthetic rate under the three electric field treatments. The +HVEF group had the highest photosynthetic rate due to enhanced $CO_2$ uptake through open stomata and an accelerated electron transport chain, increasing ATP and NADPH synthesis, thereby boosting $CO_2$ assimilation[59–61]. Figure 13(d) shows that intracellular $CO_2$ concentration was lower in the +HVEF group, indicating rapid $CO_2$ fixation for carbon assimilation, consistent with the increased photosynthetic rate. In contrast, the −HVEF and CK groups had higher intracellular $CO_2$ concentrations, likely due to lower stomatal conductance restricting $CO_2$ availability or insufficient enzymatic activity preventing efficient $CO_2$ use[58]. Figure 13(e) depicts transpiration rates, which were higher under +HVEF treatment, indicating increased stomatal opening facilitated water vapor loss. However, water-use efficiency decreased under +HVEF treatment Fig. 13(f), possibly because the simultaneous increase in photosynthesis and transpiration led to relatively lower water-use efficiency. Conversely, the −HVEF and CK groups had higher water-use efficiency, particularly the CK group[62,63]. However, this was likely due to reduced stomatal opening and restricted photosynthesis rather than an inherently higher efficiency in water use.

Additionally, Fig. 14 illustrates the diurnal variation in net photosynthetic rate across different cultivation days, all treatment groups had clear day-night fluctuations. From days 1–5, photosynthetic activity remained low, likely due to

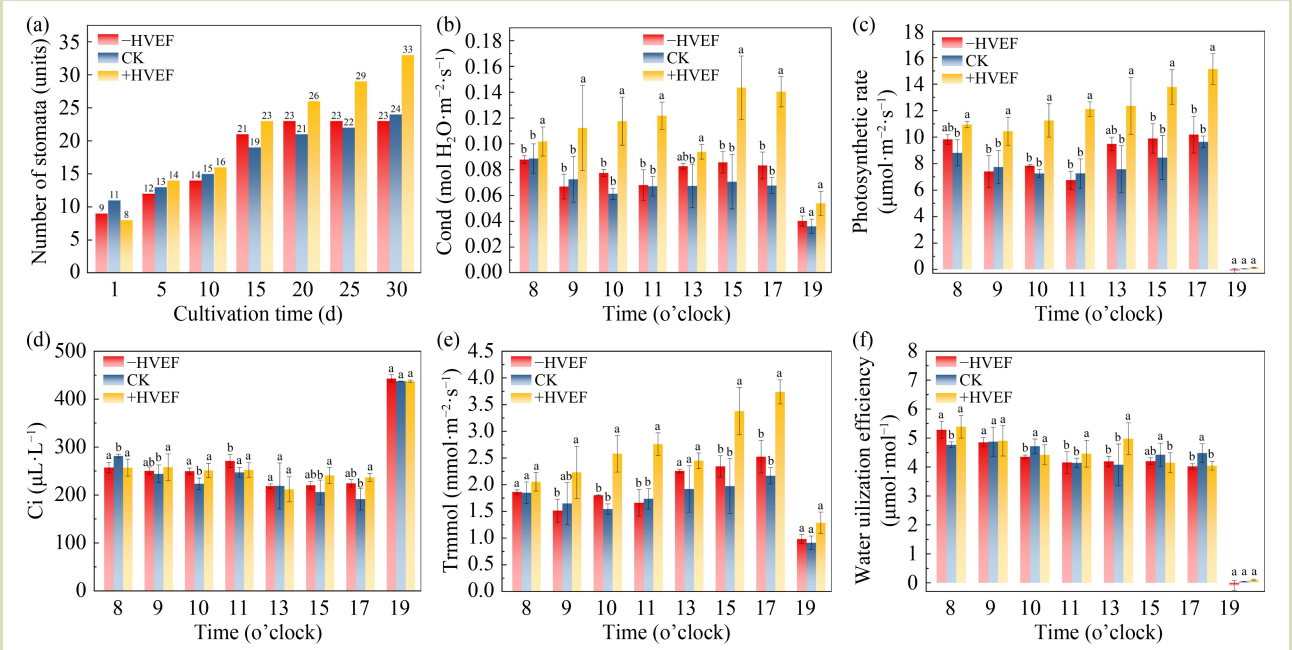


**Fig. 13** (a) Number of stomatal, (b) stomatal conductance, (c) photosynthetic rate, (d) intracellular $CO_2$ concentration, (e) transpiration rate, and (f) water-use efficiency. −HVEF, negative high-voltage electric field; CK, no electric field; and +HVEF, positive high-voltage electric field. Means with the same letters are not significantly different ($p > 0.05$) between treatments at the same time point.

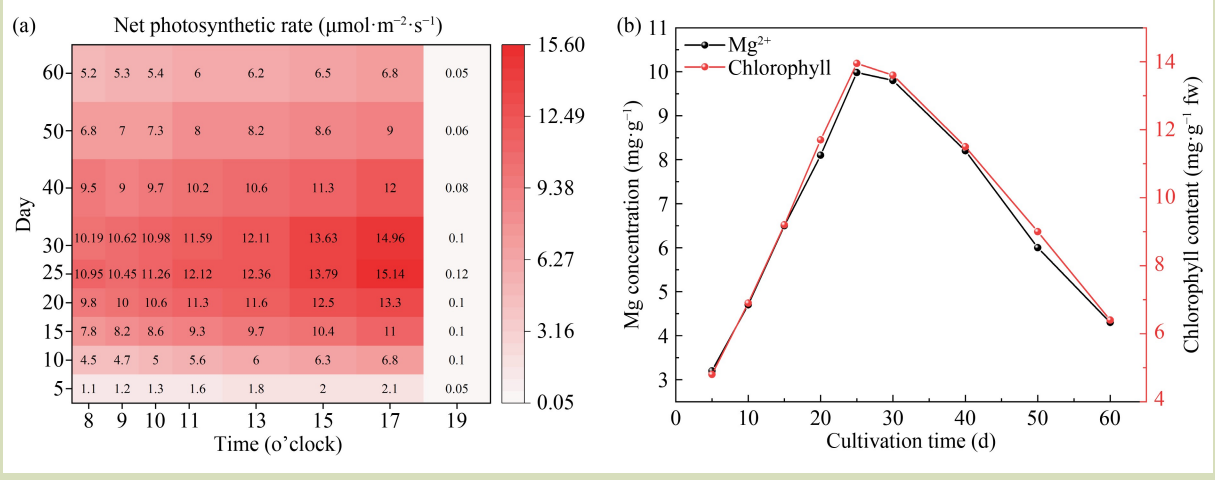


**Fig. 14** (a) Net photosynthetic rate, and (b) $Mg^{2+}$ and total chlorophyll content of tomato seedlings grown under positive high-voltage electric field after cultivation for 5–60 d.

incomplete leaf expansion during early germination. Between days 5 and 25, net photosynthetic rate progressively increased with plant age, this trend correlates with the increasing $Mg^{2+}$ content induced by +HVEF, which enhances chlorophyll biosynthesis and, consequently, photosynthetic efficiency. After day 40, a gradual decline in photosynthetic performance

was observed, possibly due to leaf senescence or reduced metabolic activity in older tissues.

As shown in Fig. 15, the activities of photosynthetic enzymes were significantly enhanced under +HVEF treatment[36], which may be attributed to accelerated transport of organic and inorganic ions from roots to leaves under +HVEF. Additionally, increased chlorophyll content under +HVEF improved light harvesting, further supporting photosynthetic efficiency through synergistic effects with enzymatic activity[36]. Also, +HVEF-induced increases in foliar $Mg^{2+}$ concentration may have contributed to enhanced photosynthesis through multiple pathways. First, $Mg^{2+}$ serves as the central coordinating ion in the chlorophyll molecule, and its sufficiency ensures efficient chlorophyll biosynthesis and light energy capture[64]. Second, $Mg^{2+}$ is essential for activating rubisco, which in turn contributes to the improvement of photosynthetic efficiency.

As shown in Figs. 13–15, +HVEF treatment significantly increased stomatal conductance and net photosynthetic rate, while the intercellular $CO_2$ concentration remained largely unchanged. This indicates that +HVEF not only enhanced stomatal aperture but also concurrently improved $CO_2$ diffusion efficiency within mesophyll tissues and carbon assimilation capacity. Typically, an increase in stomatal conductance without a corresponding rise in the net photosynthetic rate would lead to an increase in intercellular $CO_2$ concentration due to insufficient $CO_2$ fixation. However, it was stable under +HVEF indicating that the rate of $CO_2$ consumption matched the increased influx, implying a coordinated enhancement in Calvin-Benson cycle activity. This

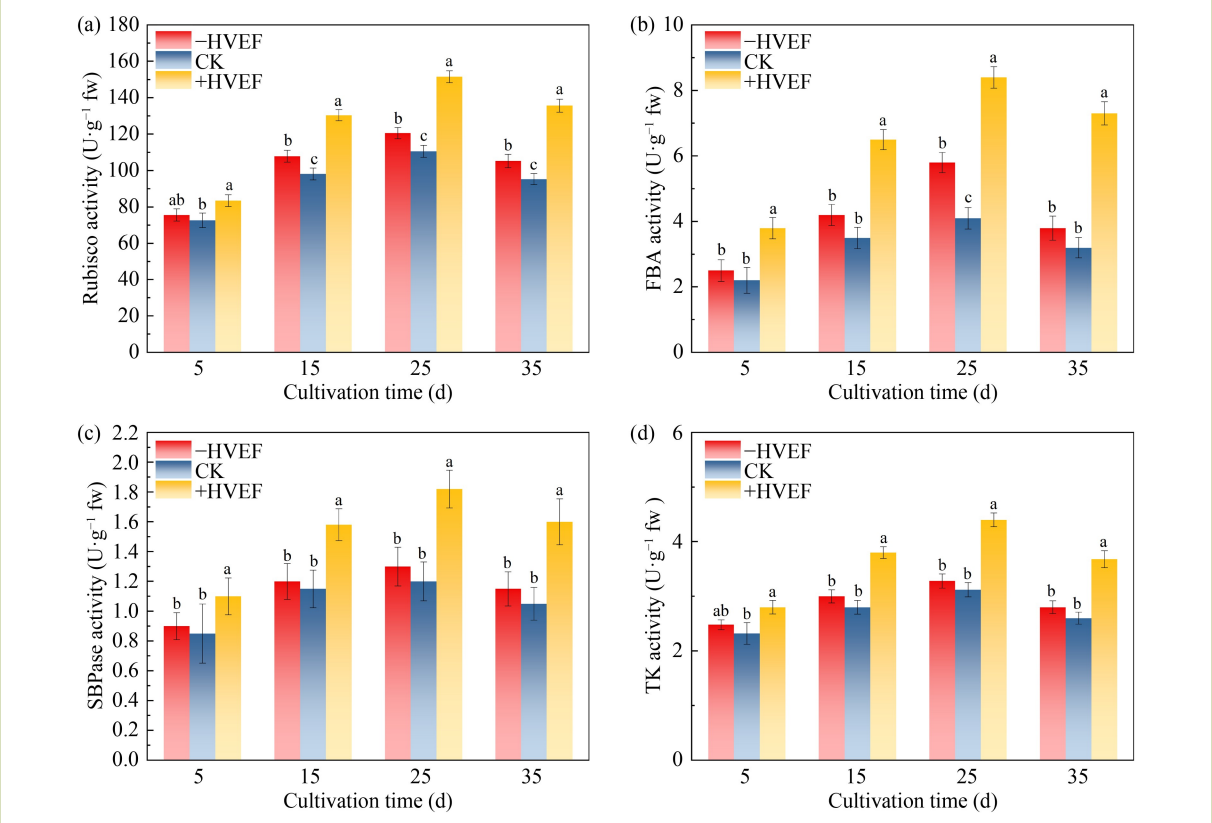


**Fig. 15** (a) Rubisco (ribulose-1,5-bisphosphate carboxylase/oxygenase), (b) FBA (fructose-1,6-bisphosphate aldolase), (c) SBPase (sedoheptulose-1,7-bisphosphatase) and (d)TK (transketolase) enzyme activities of tomato seedling leave under three electrostatic field treatments and four cultivation durations. −HVEF, negative high-voltage electric field; CK, no electric field; and +HVEF, positive high-voltage electric field. Means with the same letters are not significantly different ($p > 0.05$) between treatments at the same time point.

coordination may be attributed to the upregulation of key Calvin cycle enzymes rubisco, SBPase, FBA and TK under +HVEF treatment[36,65]. Rubisco, as the primary enzyme responsible for $CO_2$ fixation, had increased activity, accelerating carboxylation efficiency in chloroplasts and maintaining low $CO_2$ concentrations in the chloroplastic intermembrane space. Also, SBPase and FBA, which regulate the regeneration of rubisco substrates, were also activated under +HVEF, supporting an overall increase in Calvin cycle capacity. In parallel, the observed trends in $Mg^{2+}$ and chlorophyll content further support this interpretation. By day 25, the +HVEF group had a leaf $Mg^{2+}$ concentration of 9.98 $mg \cdot g^{-1}$ and a total chlorophyll content of 14.0 $mg \cdot g^{-1}$. This indicates that +HVEF not only promoted $Mg^{2+}$ accumulation in leaf tissue but may also have enhanced chlorophyll biosynthesis and the efficiency of the light reaction system.

## 4 Conclusions

This study demonstrated the effects of +HVEF on the phenotypic traits, dielectric and mesoscopic properties, ionic composition, mechanical performance and photosynthetic efficiency of tomato plants. The results reveal that +HVEF significantly enhances the uptake of key nutrients, particularly $Mg^{2+}$, leading to increased chlorophyll content and improved photosynthetic activity. By regulating membrane potential, ion channel activity and charge conduction, +HVEF promotes cell expansion and magnesium transport, thereby strengthening tissue mechanics and enhancing photosynthetic performance. Microscopic observations further confirm cell wall reinforcement and improved tissue organization. Comprehensive electrical characterization reveals that +HVEF facilitates the coupling of electrophysiological responses with photosynthesis by promoting ion transport and electrical signal conduction. The +HVEF-induced membrane hyperpolarization facilitated ion transport and stomatal regulation, thereby enhancing photosynthetic enzyme activity and supporting sustained biomass growth. These findings provide valuable insights for enhancing plant growth and advancing the application of HVEF in agricultural engineering.

### Acknowledgements

This work was funded by Introduction of Talents Research Initiation Project of Shanxi Agricultural University, China (2021BQ113).

### Compliance with ethics guidelines

Ruijie Xie, Yanbo Song, Xiaojing Shi, Liyan Jia, and Zhenyu Liu declare that they have no conflicts of interest or financial conflicts to disclose. This article does not contain any studies with human or animal subjects performed by any of the authors.

## REFERENCES

1. Sato H, Mizoi J, Shinozaki K, Yamaguchi-Shinozaki K. Complex plant responses to drought and heat stress under climate change. *Plant Journal*, 2024, **117**(6): 1873–1892
2. Naim R M, Mutalib M A, Shamsuddin A S, Lani M N, Ariffin I A, Tang S G H. Navigating the environmental, economic and social impacts of sustainable agriculture and food systems: a review. *Frontiers of Agricultural Science and Engineering*, 2024, **11**(4): 652–673
3. Yang Y, Tilman D, Jin Z, Smith P, Barrett C B, Zhu Y G, Burney J, D'Odorico P, Fantke P, Fargione J, Finlay J C, Rulli M C, Sloat L, Jan van Groenigen K, West P C, Ziska L, Michalak A M, Lobell D B, Clark M, Colquhoun J, Garg T, Garrett K A, Geels C, Hernandez R R, Herrero M, Hutchison W D, Jain M, Jungers J M, Liu B, Mueller N D, Ortiz-Bobea A, Schewe J, Song J, Verheyen J, Vitousek P, Wada Y, Xia L, Zhang X, Zhuang M. Climate change exacerbates the environmental impacts of agriculture. *Science*, 2024, **385**(6713): eadn3747
4. Croce R, Carmo-Silva E, Cho Y B, Ermakova M, Harbinson J, Lawson T, McCormick A J, Niyogi K K, Ort D R, Patel-Tupper D, Pesaresi P, Raines C, Weber A P M, Zhu X G. Perspectives on improving photosynthesis to increase crop yield. *Plant Cell*, 2024, **36**(10): 3944–3973
5. Wang Y, Liu Y, Liu X, Tang H, Huang F. Effect of plasma and electrostatic field on the growth and nutrients of Chinese cabbage. *IEEE Transactions on Plasma Science*, 2022, **50**(4): 835–840
6. Ma H, Wang L, Ke H, Zhou W, Jiang C, Jiang M, Zhan F, Li T.

Effects, physiological response and mechanism of plant under electric field application. *Scientia Horticulturae*, 2024, **329**: 112992

7. Ries A, Benítez J V, Samudio A, Armoa R, Nakayama H D. Germination of bean seeds (*Vigna unguiculata* L. Walp.) in strong electric fields. *MethodsX*, 2023, **11**: 102490
8. Li M, Wu Y, Zhang M, Zhu J. High-voltage electrostatic fields increase nitrogen uptake and improve growth of tomato seedlings. *Canadian Journal of Plant Science*, 2018, **98**(1): 93–106
9. Zhang L, Zhang M, Mujumdar A S, Ma Y. Intermittent high voltage electrostatic field and static magnetic field assisted modified atmosphere packaging alleviate mildew of postharvest strawberries after simulated transportation by activating the phenylpropanoid pathway. *Food Chemistry*, 2024, **434**: 137444
10. Sun S, Hu B, Ma J, Luo X, Guo M, Li J, Xu L, Xu X. Research on seedling sowing method based on high voltage electrostatic characteristics. *Computers and Electronics in Agriculture*, 2024, **220**: 108850
11. Hu C, Duan S, Zhou J, Yu J. Characteristics of herbivory/wound-elicited electrical signal transduction in tomato. *Frontiers of Agricultural Science and Engineering*, 2021, **8**(2): 292–301
12. Thrivikraman G, Boda S K, Basu B. Unraveling the mechanistic effects of electric field stimulation towards directing stem cell fate and function: a tissue engineering perspective. *Biomaterials*, 2018, **150**: 60–86
13. O'Shea P, Walters J, Ridge I, Wainright M, Trinci A P J. *Zeta* potential measurements of cell wall preparations from *Regnellidium diphyllum* and *Nymphoides peltata*. *Plant, Cell & Environment*, 1990, **13**(5): 447–454
14. Li J, Zhang W, Zhou H, Yu C, Li Q. Weed detection in soybean fields using improved YOLOv7 and evaluating herbicide reduction efficacy. *Frontiers in Plant Science*, 2024, **14**: 1284338
15. Wu X, Sun S, Hu B, Luo X, Li X, Han C. A study on the macro and micro mechanisms of cotton seedling growth regulation by high-voltage electrostatic field and optimization of system parameters. *Scientific Reports*, 2024, **14**(1): 30000
16. Dukic E, Herdean A, Cheregi O, Sharma A, Nziengui H, Dmitruk D, Solymosi K, Pribil M, Spetea C K. $K^+$ and $Cl^-$ channels/transporters independently fine-tune photosynthesis in plants. *Scientific Reports*, 2019, **9**(1): 8639
17. Liu W, Khan S, Tong M, Hu H, Yin L, Huang J. Identification and expression of the *CorA*/MRS2/ALR type magnesium transporters in tomato. *Plants*, 2023, **12**(13): 2512
18. Komenda J, Sobotka R, Nixon P J. The biogenesis and maintenance of PSII: recent advances and current challenges. *Plant Cell*, 2024, **36**(10): 3997–4013
19. Sauter N K, Echols N, Adams P D, Zwart P H, Kern J, Brewster A S, Koroidov S, Alonso-Mori R, Zouni A, Messinger J, Bergmann U, Yano J, Yachandra V K. No observable conformational changes in PSII. *Nature*, 2016, **533**(7603): E1–E2
20. Zhao C, Haigh A M, Holford P, Chen Z H. Roles of chloroplast retrograde signals and ion transport in plant drought tolerance. *International Journal of Molecular Sciences*, 2018, **19**(4): 963
21. Herdean A, Teardo E, Nilsson A K, Pfeil B E, Johansson O N, Ünnep R, Nagy G, Zsiros O, Dana S, Solymosi K, Garab G, Szabó I, Spetea C, Lundin B. A voltage-dependent chloride channel fine-tunes photosynthesis in plants. *Nature Communications*, 2016, **7**(1): 11654
22. Lunin V V, Dobrovetsky E, Khutoreskaya G, Zhang R, Joachimiak A, Doyle D A, Bochkarev A, Maguire M E, Edwards A M, Koth C M. Crystal structure of the *CorA* $Mg^{2+}$ transporter. *Nature*, 2006, **440**(7085): 833–837
23. Sukhova E M, Yudina L M, Sukhov V S. Changes in activity of the plasma membrane $H^+$-ATPase as a link between formation of electrical signals and induction of photosynthetic responses in higher plants. *Biochemistry*, 2023, **88**(10): 1488–1503
24. Kozlova E, Yudina L, Sukhova E, Sukhov V. Analysis of electrome as a tool for plant monitoring: progress and perspectives. *Plants*, 2025, **14**(10): 1500
25. Lee S, Oh M M. Electrocultivation of *Arabidopsis thaliana* increases water and mineral absorption, electric charge and auxin accumulation, enhancing growth and development. *Bioelectrochemistry*, 2025, **163**: 108893
26. Attri P, Okumura T, Koga K, Shiratani M, Wang D, Takahashi K, Takaki K. Outcomes of pulsed electric fields and nonthermal plasma treatments on seed germination and protein functions. *Agronomy*, 2022, **12**(2): 482
27. Song J, Zhang R, Yang F, Wang J, Cai W, Zhang Y. Nocturnal LED supplemental lighting improves quality of tomato seedlings by increasing biomass accumulation in a controlled environment. *Agronomy*, 2024, **14**(9): 1888
28. Colman S L, Salcedo M F, Mansilla A Y, Iglesias M J, Fiol D F, Martín-Saldaña S, Alvarez V A, Chevalier A A, Casalongué C A. Chitosan microparticles improve tomato seedling biomass and modulate hormonal, redox and defense pathways. *Plant Physiology and Biochemistry*, 2019, **143**: 203–211
29. Cotta F C, Amaral R, Bacellar F L, Correia D, Asadi K, Rocha P R F. A 3D porous electrode for real-time monitoring of microalgal growth and exopolysaccharides yields using Electrochemical Impedance Spectroscopy. *Biosensors & Bioelectronics*, 2025, **277**: 117260
30. Fahimi P, Castanedo L A M, Vernier P T, Matta C F. Electrical homeostasis of the inner mitochondrial membrane potential. *Physical Biology*, 2025, **22**(2): 026001
31. Shakibi R, Yazdipour F, Abadijoo H, Manoochehri N, Rostami Pouria F, Bajooli T, Simaee H, Abdolmaleki P, Khatibi A, Abdolahad M, Moosavi-Movahhedi A A, Ali Khayamian M. From resting potential to dynamics: advances in membrane

voltage indicators and imaging techniques. *Quarterly Reviews of Biophysics*, 2025, **58**: e7

32. Figueiredo A S, Sánchez-Loredo M G, de Pinho M N, Minhalma M. Surface-charge characterization of nanocomposite cellulose acetate/silver membranes and BSA permeation performance. *Membranes*, 2025, **15**(2): 61
33. Kumar J, Das Gupta P, Ghosh S. The role of nonlinear axonal membrane capacitance in modulating ion channel cooperativity in action potential dynamics: studies on Hodgkin-Huxley's model. *Biophysical Chemistry*, 2025, **319**: 107391
34. Szabo M, Cs Szabo B, Kurtan K, Varga Z, Panyi G, Nagy P, Zakany F, Kovacs T. Look beyond plasma membrane biophysics: revealing considerable variability of the dipole potential between plasma and organelle membranes of living cells. *International Journal of Molecular Sciences*, 2025, **26**(3): 889
35. Niitsu A, Jung J, Sugita Y. Structural dynamics of a designed peptide pore under an external electric field. *Biophysical Chemistry*, 2025, **318**: 107380
36. Wang D, Hayashi Y, Enoki T, Nakahara K, Arita T, Higashi Y, Kuno Y, Terazawa T, Namihira T. Influence of pulsed electric fields on photosynthesis in light/dark-acclimated lettuce. *Agronomy*, 2022, **12**(1): 173
37. Xu W, Song Z, Luan X, Ding C, Cao Z, Ma X. Biological effects of high-voltage electric field treatment of naked oat seeds. *Applied Sciences*, 2019, **9**(18): 3829
38. Hamilton D W, Hills A, Kohler B, Blatt M R. $Ca^{2+}$ channels at the plasma membrane of stomatal guard cells are activated by hyperpolarization and abscisic acid. *Proceedings of the National Academy of Sciences of the United States of America*, 2000, **97**(9): 4967–4972
39. Jezek M, Blatt M R. The membrane transport system of the guard cell and its integration for stomatal dynamics. *Plant Physiology*, 2017, **174**(2): 487–519
40. Saletnik B, Zaguła G, Saletnik A, Bajcar M, Słysz E, Puchalski C. Effect of magnetic and electrical fields on yield, shelf life and quality of fruits. *Applied Sciences*, 2022, **12**(6): 3183
41. Dong Z, Feng L, Liu Z, Zhao J, Wang J, Zhang M. Study on the correlation between water content of peanut kernel, water phase state and electrical impedance spectrum parameters. *Journal of Food Process Engineering*, 2025, **48**(2): e70057
42. Volkov A G. Green plants: electrochemical interfaces. *Journal of Electroanalytical Chemistry*, 2000, **483**(1–2): 150–156
43. Wang Y, Wu H, Geng Y, Zhang Z, Fu J, Ouyang J, Zhu Z. Equivalent circuit modeling and analysis for microfluidic electrical impedance monitoring of single-cell growth. *Biosensors*, 2025, **15**(2): 113
44. Dikbaş N, Alım Ş, Uçar S, Çepni E. Immobilization of mannanase enzyme to ZnO nanoparticle and determination of its effect on tomato seed germination. *Journal of Soil Science and Plant Nutrition*, 2023, **23**(4): 5683–5694
45. Zhang X, Xia C, Liu W, Hao M, Miao Y, Gao F. Microwave absorption and thermal properties of coral-like SiC aerogel composites prepared by water glass as a silicon source. *International Journal of Minerals Metallurgy and Materials*, 2023, **30**(7): 1375–1387
46. Huang B, Li S, Long T, Bai S, Zhao J, Xu H, Lan Y, Liu H, Long Y. Research on predicting photosynthetic pigments in tomato seedling leaves based on near-infrared hyperspectral imaging and machine learning. *Microchemical Journal*, 2024, **204**: 111076
47. Unal D, Gurbanov R, Sevim G, Samgane G, Varış G, Ozdemir-Kocak F, Tuney-Kizilkaya I. Dose-dependent plant-promoting effect of macroalgae *Stypopodium schimperi* extracts in *Solanum lycopersicum* and detection of phloroglucinol composition. *Journal of Soil Science and Plant Nutrition*, 2023, **23**(2): 2018–2029
48. Wang Y, Liu Q, Shao Z, Wang X S, Chen Y F, Bai J J, Chen M L, Wang J H. Investigation on effects of $TiO_2$ on cucumber seedlings using ICP-OES and LA-ICP-MS. *Analytica Chimica Acta*, 2025, **1352**: 343917
49. Schock I, Gregan J, Steinhauser S, Schweyen R, Brennicke A, Knoop V. A member of a novel *Arabidopsis thaliana* gene family of candidate $Mg^{2+}$ ion transporters complements a yeast mitochondrial group II intron-splicing mutant. *Plant Journal*, 2000, **24**(4): 489–501
50. Ishijima S, Manabe Y, Shinkawa Y, Hotta A, Tokumasu A, Ida M, Sagami I. The homologous *Arabidopsis* MRS2/MGT/CorA-type $Mg^{2+}$ channels, AtMRS2–10 and AtMRS2–1 exhibit different aluminum transport activity. *Biochimica et Biophysica Acta Biomembranes (BBA) - Biochimica et Biophysica Acta. Biomembranes*, 2018, **1860**(11): 2184–2191
51. Li L, Tutone A F, Drummond R S, Gardner R C, Luan S. A novel family of magnesium transport genes in *Arabidopsis*. *Plant Cell*, 2001, **13**(12): 2761–2775
52. Kaplan B, Sherman T, Fromm H. Cyclic nucleotide-gated channels in plants. *FEBS Letters*, 2007, **581**(12): 2237–2246
53. Palmgren M G. PLANT PLASMA MEMBRANE $H^+$-ATPases: powerhouses for nutrient uptake. *Annual Review of Plant Physiology and Plant Molecular Biology*, 2001, **52**(1): 817–845
54. Regmi S, Janaswamy S. Biodegradable packaging films from the alkali-extracted lignocellulosic residue of soyhulls extend the shelf life of strawberries. *Food Bioscience*, 2025, **65**: 106016
55. Liu S, Jin Z, Zhou P, Shang H, Yang H, Li L, Li R, Zhang Y, Chen H. Preparation of wheat-straw-fiber-based degradable mulch film for sustained release of carbendazim and its application for soybean root rot control. *Agronomy*, 2025, **15**(1): 71
56. Massimi M, Radócz L, Kabashi B. The response of chlorophyll content and ionic composition in tomato and pepper seedlings to foliar nutrition in growing chambers. *Agronomy*, 2023,

**13**(9): 2234

57. Chauhan D K, Yadav V, Vaculík M, Gassmann W, Pike S, Arif N, Singh V P, Deshmukh R, Sahi S, Tripathi D K. Aluminum toxicity and aluminum stress-induced physiological tolerance responses in higher plants. *Critical Reviews in Biotechnology*, 2021, **41**(5): 715–730
58. Hanson D T, Stutz S S, Boyer J S. Why small fluxes matter: the case and approaches for improving measurements of photosynthesis and (photo)respiration. *Journal of Experimental Botany*, 2016, **67**(10): 3027–3039
59. Witt H T. Energy conversion in the functional membrane of photosynthesis. Analysis by light pulse and electric pulse methods. The central role of the electric field. *Biochimica et Biophysica Acta* (*BBA*) - *Reviews on Bioenergetics*, 1979, **505**(3–4): 355–427
60. Tahi H, Wahbi S, Wakrim R, Aganchich B, Serraj R, Centritto M. Water relations, photosynthesis, growth and water-use efficiency in tomato plants subjected to partial rootzone drying and regulated deficit irrigation. *Plant Biosystems - an International Journal Dealing with All Aspects of Plant Biology*, 2007, **141**(2): 265–274
61. Liu H, Zheng Z, Han X, Zhang C, Li H, Wu M. Chitosan soaking improves seed germination of *Platycodon grandiflorus* and enhances its growth, photosynthesis, resistance, yield, and quality. *Horticulturae*, 2022, **8**(10): 943
62. Leakey A D B, Ferguson J N, Pignon C P, Wu A, Jin Z, Hammer G L, Lobell D B. Water use efficiency as a constraint and target for improving the resilience and productivity of $C_3$ and $C_4$ crops. *Annual Review of Plant Biology*, 2019, **70**(1): 781–808
63. Schulze E D, Kelliher F M, Korner C, Lloyd J, Leuning R. Relationships among maximum stomatal conductance, ecosystem surface conductance, carbon assimilation rate, and plant nitrogen nutrition: a global ecology scaling exercise. *Annual Review of Ecology and Systematics*, 1994, **25**(1): 629–662
64. Shao Y, Li S, Gao L, Sun C, Hu J, Ullah A, Gao J, Li X, Liu S, Jiang D, Cao W, Tian Z, Dai T. Magnesium application promotes rubisco activation and contributes to high-temperature stress alleviation in wheat during the grain filling. *Frontiers in Plant Science*, 2021, **12**: 675582
65. Michelet L, Zaffagnini M, Morisse S, Sparla F, Pérez-Pérez M E, Francia F, Danon A, Marchand C H, Fermani S, Trost P, Lemaire S D. Redox regulation of the Calvin-Benson cycle: something old, something new. *Frontiers in Plant Science*, 2013, **4**: 470